Lab on a Chip

RSC Publishing

COMMUNICATION

View Article Online
View Journal | View Issue

Cite this: *Lab Chip*, 2013, **13**, 4160

Received 16th May 2013,
Accepted 5th August 2013

DOI: 10.1039/c3lc50571e

www.rsc.org/loc

A novel approach to quantifying ciliary physiology: microfluidic mixing driven by a ciliated biological surface†

Stephan Jonas,*[ab] Elaine Zhou,[ac] Engin Deniz,[d] Brendan Huang,[c] Kenny Chandrasekera,[c] Dipankan Bhattacharya,[d] Yu Wu,[c] Rong Fan,[c] Thomas M. Deserno,[b] Mustafa K. Khokha[de] and Michael A. Choma*[acd]

From the lungs to the central nervous system, cilia-driven fluid flow plays a fundamental role in many facets of life. Yet, there are few quantitative methods for analysing the function of ciliated surfaces. Here, we report a novel microfluidic approach for quantifying the performance of a ciliated surface using mixing performance as an integrated readout.

Motile cilia are cellular projections that drive microfluidic flow across different biological surfaces. Cilia generate directional flow by executing a periodic, asymmetric beat pattern consisting of a forward power stroke and a return stroke.[1,2] Cilia-driven fluid flow is critical to the normal functioning of several different organ systems, (*e.g.* cerebrospinal fluid flow in the central nervous system,[3] mucous transport in the respiratory system[4]). Defects in cilia-driven fluid flow lead to several different disease states including recurrent lung infections in primary ciliary dyskinesia and cystic fibrosis.[2,4] Abnormal cilia-driven fluid flow also is implicated in the etiology of heterotaxy syndrome, a disease with left-right axis defects resulting in severe heart and other thoraco-abdominal defects.[5,6] Nevertheless, quantification of cilia-driven fluid flow remains a challenge. The analysis of ciliary beat frequency or ciliary ultrastructure is limited in that it does not directly quantify physiological flow performance. Moreover, the patterning of a ciliary surface also can alter flow, even in the setting of otherwise normal cilia.[7] The canonical approach for quantifying cilia-driven fluid flow relies on flow velocimetry. Historically, most flow velocimetry approaches have been semi-quantitative because they employ microscopy methods that are not cross-sectional in nature, meaning that information was integrated across the optical axis of the microscope. More recent methods[8–10] employ cross-sectional imaging to generate spatially resolved flow velocity measurements. These spatially resolved flow vector maps that quantitatively describe the flow field can be further processed to give one or several diagnostic readouts. Even though velocimetry is an active area of research, new kinds of diagnostic readouts might be of interest that directly exploit the microfluidic nature of cilia-driven fluid flow.

Prior work has recognized that cilia can drive microfluidic mixing.[11–15] Two general mechanisms have been demonstrated. First, cilia can drive near-field mixing through enhanced diffusion, that is, an apparent particle diffusivity measured near individual cilia that is larger than otherwise expected.[11,14,15] Enhanced near-field diffusion can occur in the setting of either uncoordinated[11,15] or coordinated ciliary beating.[14] Second, far-field directional flow driven by the coordinated beating of cilia can be exploited to drive mixing when the flow is confined to specifically designed geometries.[11–13] Indeed, our prior work demonstrated that a biological ciliated surface can drive mixing-type flow patterns.[8] Such patterns are reminiscent of mixing driven by biomimetic cilia.[12,13] This similarity inspired us to develop a new kind of quantitative readout for biological ciliary flow performance: microfluidic mixing efficiency. Our novel approach is to use a ciliated biological surface as a microfluidic "component" and to design microfluidic chips and imaging strategies to quantify the performance of that component. To that end, we designed a polydimethylsiloxane (PDMS) chip to allow for the delivery of tracer dye into a chamber containing a ciliated surface. We used colour videomicroscopy on a consumer-grade DSLR camera (Canon EOS D5 Mark II) and a standard stereomicroscope to capture cilia-driven dye mixing. We used two distinct image-processing strategies (Shannon information entropy and dye frontline tracking) to quantify mixing efficiency. Finally, we demonstrated our conceptually new approach by quantifying reduced cilia-driven mixing performance in the setting of increased fluid viscosity.

We chose *Xenopus* (tadpole) embryos as our animal model since they are an important model organism in vertebrate ciliary biology.[16] Like other amphibian embryos, the skin of *Xenopus* embryos is ciliated[17] (Fig. 1) The ciliated skin drives flow that

[a]*Dept. of Diagnostic Radiology, Yale University, New Haven, CT, USA. E-mail: michael.choma@yale.edu; Tel: +1 (203) 785-2945*
[b]*Dept. of Medical Informatics, RWTH Aachen University, Pauwelsstr. 30, Aachen, Germany. E-mail: sjonas@mi.rwth-aachen.de; Fax: +49 241 803388795; Tel: +49 241 8088795*
[c]*Dept. of Biomedical Engineering, Yale University, New Haven, CT, USA*
[d]*Dept. of Pediatrics, Yale University, New Haven, CT, USA*
[e]*Dept. of Genetics, Yale University, New Haven, CT, USA*

† Electronic supplementary information (ESI) available. See DOI: 10.1039/c3lc50571e

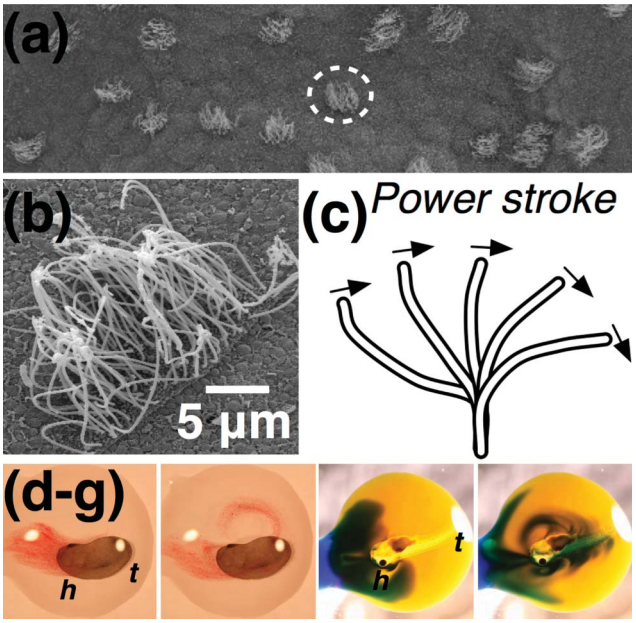

Fig. 1 (a) Scanning electron micrograph (SEM) of *Xenopus* embryo skin showing multiciliated cells. The dashed circle highlights a ciliated cell. (b) Higher magnification SEM of a multiciliated cell. (c) Schematic of the forward power stroke of an individual cilia, adapted from ref. 2. The direction of the power stroke determines flow direction. (d–g) Qualitative demonstrations of cilia-driven microfluidic mixing. (d–e) show a NF stage 25 embryo in a drop of water. The ciliated skin drives mixing of red microspheres. There is surface flow in a head-to-tail direction as well as a tail-to-head recirculatory flow (arrowheads; Movie 1†). (f–g) show a NF stage 41 embryo in a yellow dye solution. Cilia-driven flow drives mixing of a blue dye with the yellow, leading to a green colour readout (Movie 2†). *h*, head; *t*, tail.

generates mixing in close proximity to the embryo (Fig. 1b–f). In our experiments, we only used morphologically normal embryos. Fig. 1d–e and Movie 1† show a Nieuwkoop-Faber (NF) stage 25 embryo in a transparent drop of physiological solution. The ciliated skin drives mixing of a red microsphere solution. There is surface flow in a head-to-tail direction with a tail-to-head recirculatory flow further away from the surface. Fig. 1f–g and Movie 2† show a NF stage 41 embryo in a yellow dye-coloured physiological solution. Here, cilia-driven flow drives mixing of a blue dye with a yellow dye, leading to a green colour readout.

While our initial mixing work demonstrated the principle of using a ciliated biological surface to drive microfluidic mixing, the approach of confining the surface in an arbitrary drop of fluid had significant limitations. Importantly, it was prohibitively difficult to generate the same drop shape between experiments and to manually deliver flow contrast agent in a reproducible manner using a micropipette. We therefore designed a microfluidic chip to overcome these limitations and to move from a qualitative demonstration to a quantitative assay. Using a do-it-yourself method,[18] an initial prototype was developed (Movie 3†). Our final PDMS chip design is composed of two inflow channels, one outflow channel, and a suction channel (Fig. 2, ESI†). The chip meets the following specifications: (i) controlled delivery of flow contrast agent; (ii) multiple inflow channels for contrast agent, drugs, and physiological solution; (iii) single outflow channel that

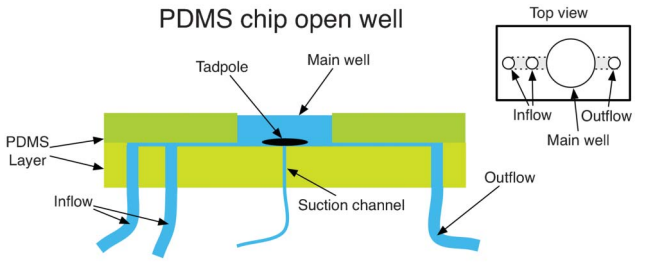

Fig. 2 A schematic of the PDMS microfluidic chip.

enables coordinated, simultaneous inflow and outflow of mixing well fluid; (iv) gentle securing of ciliated embryos *via* suction; and (v) reusability of the well.

Since the mixing chamber geometry influences mixing patterns, a cylindrical well was used. Given a typical embryo thickness of ~0.5 mm, a cylinder height of 1 mm completely immerses the embryo in physiological solution. At a height of 1 mm, there is insufficient distance between the ciliated surface and the air/water interface for a recirculatory mixing flow to form above the embryo. The well radius of 3 mm was set by the minimum distance between the embryo body and well wall needed to establish recirculatory mixing flow in the plane orthogonal to the optical axis of the imaging microscope. In our experience, this distance is approximately 1 body length.[8] That is, the chip is designed to generate mixing along the dorsal (back) and ventral (front/abdomen) aspects of the embryo. Note that, since recirculatory flow is expected only orthogonal to the optical axis, we expect to minimize dye concentration variability along the projection axis of our two-dimensional imaging.

Two methods for quantifying mixing efficiency are demonstrated: (i) Shannon information entropy, a measure of disorder in a digital signal that has been previously used in microfluidic mixing quantification,[19] and (ii) frontline tracking, a measure of time-varying geometric properties of the dye/fluid interface.

Mixing can be seen as a disordering or randomization process. Thus, Shannon information entropy[20] H is a natural measurement of mixing performance. Shannon information entropy H is defined as $H = -\Sigma[p(x)\log_2(p(x))]$, where $p(x)$ is the probability density function describing a digital signal x that can exist in $i \in \{1,2,...,2^N\}$ states and N is the bit depth of the digital signal.[20] Hence, a random signal has maximum entropy $H = N$, while a signal composed of repeated elements has $H = 0$ entropy. In our case, the signals x are extracted from a digital movie recording of the cilia-driven mixing. They can be defined locally (windowed) and globally over time and space (Fig. 3). In particular, the entropy can be calculated at an individual pixel over a specified time interval δt (temporal entropy) or over a spatial region of interest at a particular moment in time (spatial entropy). Windowed temporal entropy generates M entropy maps, where $M = \Delta t/\delta t$ and Δt is the duration of a movie recording. These windowed temporal entropy maps (Fig. 4 and Movie 5†) show the time evolution of cilia-driven mixing "hot spots" and "cold spots." Time-varying spatial entropy naturally lends itself to integrated, quantitative measures of mixing performance. In particular, we

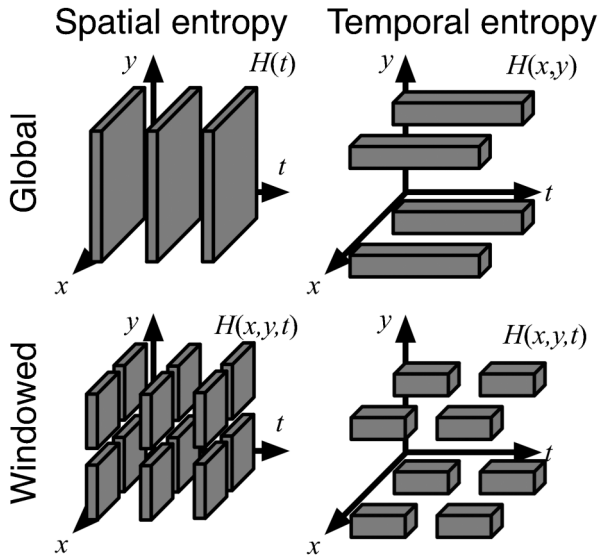

Fig. 3 Classification of Shannon information entropy measurements.

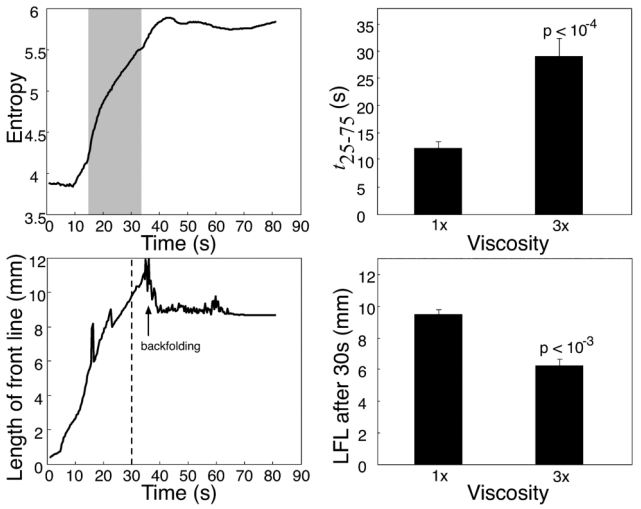

Fig. 5 Results of comparative analysis between normal and increased viscosity experiments. Error bars show standard error of the mean. t_{25-75} defines the time between 25% and 75% of maximum entropy.

found that the time duration of the curve upswing in 25% to 75% of maximum entropy (t_{25-75}) can be used as a readout for cilia driven mixing efficiency. Here, shorter t_{25-75} times indicate more efficient cilia-driven mixing. We demonstrated t_{25-75} in a biologically relevant experiment. We compared t_{25-75} times in normal and 3× fluid viscosity in NF stage 30 embryos (n = 20 embryos in 1× viscosity and n = 18 embryos in 3× viscosity). One 1× viscosity experiment was excluded owing to an entropy curve that did not peak over the course of movie acquisition. Fluid viscosity was increased using high molecular weight dextran.[21] t_{25-75} times were significantly increased by tripling the fluid viscosity ($p = 9 \times 10^{-5}$; Fig. 5), indicating that increased fluid viscosity decreases microfluidic mixing efficiency driven by the ciliated biological surface.

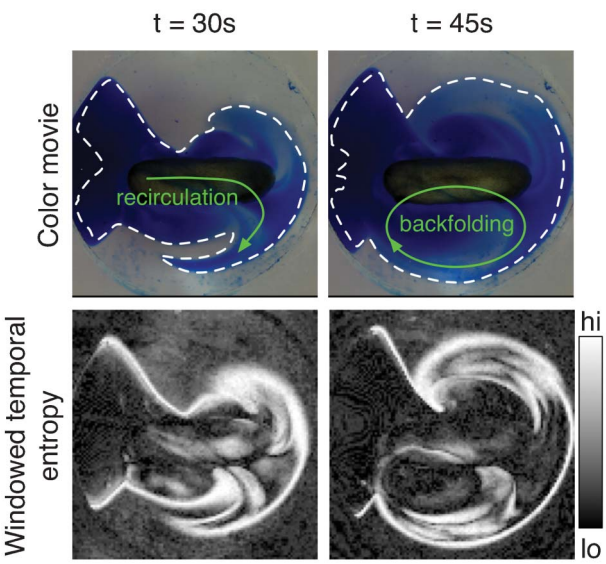

Fig. 4 Sample sequence of images and processing at different time points. Upper row shows raw images with superimposed frontline (dashed line; Movie 4†). Lower row shows windowed temporal entropy over 5 s of mixing at these time points (Movie 5†). NF stage 30.

Since there are different computational methods for quantifying mixing efficiency, we sought to demonstrate that our approach is robust to different methods. Thus, in addition to Shannon information entropy, we demonstrated frontline tracking. Frontline tracking was suggested by Khatavkar, *et al.*[12] as an alternate for quantifying mixing efficiency. Since microfluidic mixing can be thought of as stirring and diffusion, the efficiency of mixing is dependent on stirring performance.[22] One measure of stirring performance is the extent to which the interface (*i.e.* frontline) between two fluids (*e.g.* dye and transparent fluid) increases as a function of time. Here, we estimate the length of the interface between dye contrast agent and the transparent physiological solution in which the ciliated surface sits (Fig. 4). The rationale is that diffusion gradients are maximised at interfaces, and that longer interfaces promote more efficient diffusion over a more spatially distributed extent in the mixing well. We also note that, while velocimetry quantifies steady-state features of a flow field, frontline tracking quantifies non-steady-state features of a mixing process.

A frontline tracking algorithm was designed with smoothing in curvature scale space (ESI†). The same acquisitions for the above Shannon information entropy experiments were used for frontline tracking experiments (n = 21 embryos in 1× viscosity and n = 18 embryos in 3× viscosity). A threefold increase in viscosity resulted in statistically significantly shorter frontline lengths at 30 and 45 s after introduction of the dye ($p = 2 \times 10^{-4}$ and $p = 4 \times 10^{-4}$ for 30 and 45 s, respectively). Here, shorter (longer) frontline lengths at a particular time point indicate lower (higher) mixing efficiency, respectively. Frontline lengths at 60 s were not significantly different between the two viscosity groups. This lack of significance can be attributed to backfolding of recirculatory loops onto themselves. Backfolding abruptly decreases interfacial or

frontline length (Fig. 4), indicating that frontline length is useful only during the initial stages of mixing after introduction of dye into the mixing well.

In sum, we have demonstrated a conceptually novel approach to quantifying the performance of a biological ciliated surface. Our approach uses a biological ciliated surface in a microfluidic assay supported by a specifically designed PDMS microfluidic chip and quantitative image analysis. The assay yields two distinct quantitative biomarkers that reflect the integrated performance of a biological ciliated surface. In addition to demonstrating that the mixing can be reliably quantified, we showed that impairment of directional flow by increased fluid viscosity also impairs mixing efficiency, thereby making a concrete connection between biologically-relevant functioning and mixing efficiency. Integrated performance as readout by a single readout measure is of particular interest in ciliary biology since many different kinds of defects can occur in a ciliated surface, ranging from ultrastructural defects in the ciliary molecular motor to the developmental patterning of the surface. A single readout measure may be useful when an experimental or clinical question relies on knowing whether performance is normal or abnormal but direct knowledge of flow velocity is not needed. Mixing performance may have future use in a genetic screen using ciliated *Xenopus* embryos. Clinically, mixing performance may have utility in the rapid assessment of ciliated biopsy specimens (*e.g.* nasal polyps, tracheal strip biopsy). Future work also will focus on (a) understanding how different defects at different size scales modify cilia-driven mixing performance and (b) extending the present work that uses 2D projection imaging to cross-sectional and 3D imaging. Lastly, our work may advance understanding the flow in the embryonic node. The node is a transient organ that is present during early embryonic development. The floor of the node is ciliated, and directional cilia-driven flow within a well-defined geometry establishes left-right body axis orientation.[5,6,23] Using chips with custom geometries is a promising approach to elucidating relationships between flow geometry and cilia-driven fluid flow.

Acknowledgements

All research was conducted with Yale IACUC approval. RF acknowledges support from the Yale University New Faculty Startup fund and the use of equipment at Yale Nanofabrication Center and Yale Institute for Nanoscience and Quantum Engineering (YINQE). MKK acknowledges support by NIH grants 1R01DE018824 and 1R01DE018825. MAC acknowledges support through a K12 award from the Yale Child Health Research Center (5K12-HD001401-12).

References

1 E. M. Purcell, *Am. J. Phys.*, 1977, **45**, 3–11.
2 M. R. Knowles and R. C. Boucher, *J. Clin. Invest.*, 2002, **109**, 571–577.
3 J. J. Breunig, J. I. Arellano and P. Rakic, *Nat. Neurosci.*, 2010, **13**, 654–655.
4 K. Baker and P. L. Beales, *Am. J. Med. Genet., Part C*, 2009, **151C**, 281–295.
5 M. Brueckner, *Circulation*, 2007, **115**, 2793–2795.
6 M. Brueckner, *Circulation*, 2012, **125**, 2178–2180.
7 B. Mitchell, R. Jacobs, J. Li, S. Chien and C. Kintner, *Nature*, 2007, **447**, 97–101.
8 S. Jonas, D. Bhattacharya, M. K. Khokha and M. A. Choma, *Biomed. Opt. Express*, 2011, **2**, 2022–2034.
9 A. L. Oldenburg, R. K. Chhetri, D. B. Hill and B. Button, *Biomed. Opt. Express*, 2012, **3**, 1978–1992.
10 L. Liu, K. K. Chu, G. H. Houser, B. J. Diephuis, Y. Li, E. J. Wilsterman, S. Shastry, G. Dierksen, S. E. Birket, M. Mazur, S. Byan-Parker, W. E. Grizzle, E. J. Sorscher, S. M. Rowe and G. J. Tearney, *PLoS One*, 2013, **8**, e54473.
11 M. J. Kim and K. S. Breuer, *J. Fluids Eng.*, 2006, **129**, 319–324.
12 V. V. Khatavkar, P. D. Anderson, J. M. J. den Toonder and H. E. H. Meijer, *Phys. Fluids*, 2007, **19**, 083605.
13 J. den Toonder, F. Bos, D. Broer, L. Filippini, M. Gillies, J. de Goede, T. Mol, M. Reijme, W. Talen, H. Wilderbeek, V. Khatavkar and P. Anderson, *Lab Chip*, 2008, **8**, 533–541.
14 A. R. Shields, B. L. Fiser, B. A. Evans, M. R. Falvo, S. Washburn and R. Superfine, *Proc. Natl. Acad. Sci. U. S. A.*, 2010, **107**, 15670–15675.
15 K. C. Leptos, J. S. Guasto, J. P. Gollub, A. I. Pesci and R. E. Goldstein, *Phys. Rev. Lett.*, 2009, **103.**
16 M. E. Werner and B. J. Mitchell, *Genesis*, 2012, **50**, 176–185.
17 R. Assheton, *Q. J. Microsc. Sci.*, 1896, **2**, 465–484.
18 P. K. Yuen and V. N. Goral, *Lab Chip*, 2010, **10**, 384–387.
19 M. Camesasca, I. Manas-Zloczower and M. Kaufman, *J. Micromech. Microeng.*, 2005, **15**, 2038–2044.
20 C. E. Shannon, *AT&T Tech. J.*, 1948, **27**, 623–656.
21 L. Gheber, A. Korngreen and Z. Priel, *Cell Motil. Cytoskeleton*, 1998, **39**, 9–20.
22 T. M. Squires and S. R. Quake, *Rev. Mod. Phys.*, 2005, **77**, 977–1026.
23 J. H. E. Cartwright, N. Piro, O. Piro and I. Tuval, *Dev. Dyn.*, 2008, **237**, 3477–3490.